Experimental validation of finite element models representing stacked concrete beams with unbonded surface contacts

M. Filippoupolitis[1,2], C. Hopkins[1,*]

[1]Acoustics Research Unit, School of Architecture, University of Liverpool, Liverpool L69 7ZN, United Kingdom

[2]Institute for Risk and Uncertainty, University of Liverpool, Liverpool L69 7ZF, United Kingdom

* Corresponding author

Abstract

This paper investigates the dynamic behaviour of stacked reinforced concrete beams using experimental modal analysis and finite element methods. Finite element models of five different junctions were developed with surface-to-surface and edge-to-surface contact conditions between the beams. It was shown that the interaction between the beams could be approximated using a normal contact stiffness which is independent of the shape of the junction and follows a lognormal distribution. The models were experimentally validated in terms of eigenfrequencies and mode shapes. To assess the suitability of the model it was found to be essential to verify the spatial-average response. This was achieved by introducing the Partial Modal Vector Ratio (PMVR) as a supplement to the Modal Assurance Criterion (MAC) for the validation of the FEM models. PMVR is a time efficient approach to identify appropriate models and can be used as a supplementary criterion to MAC when there are correlation issues caused by the interaction of the beams.

1. Introduction

Earthquakes regularly lead to severely damaged or collapsed buildings (e.g. [1,2,3]) and a high rate of mortality [4]. For the rescue services it is necessary to quickly detect and locate survivors inside a collapsed structure [5]. Survivors sometimes knock or hit the nearest part of the collapsed structure to try and let others know that they are alive. However, the rescuers have limited experience in assessing when it is appropriate for everyone to stop digging and listen for signs of life, and distinguish them from other sources of vibration [6,7]. For this reason, prediction of vibration transmission in collapsed and fragmented reinforced-concrete buildings has the potential to inform decisions about the detection of trapped human survivors. After a reinforced concrete building has collapsed, many concrete elements are touching but they are in contact without the presence of any bonding material. This paper investigates the potential to predict vibration transmission across unbonded contacts between reinforced concrete elements.

For lightweight structural elements that are not rigidly bonded together, vibratory motion results in them being in two distinct states, in contact and out-of-contact. For example, Ervin [8] modelled impacts between two orthogonal pinned-pinned beams using an elastic spring. For fragmented, heavy, concrete elements that touch each other after a building collapse it is reasonable to assume that they will remain in contact whilst undergoing vibratory motion, and that it may also be possible to model the interaction between them using lump spring elements. Springs are useful in modelling complex connections between structural elements (e.g. [9,10,11]) and their stiffness can be determined analytically, or by model updating [12] against experimental results. For coupled beams, previous research has mainly focussed on their vibration when aligned parallel to each other and connected with uniformly distributed translational springs (e.g. [13,14,15]). Hence for the application described above there is a need to understand the dynamics of simple structural elements such as beams when connected at arbitrary angles to each other with surface-to-surface and edge-to-surface contacts.

Mode based methods in dynamics can be used to detect damage to structures [16]. However, for reinforced concrete beams or columns these only tend to focus on the first few modes of vibration

(e.g. [17,18,19]). Finite Element Methods (FEM) have been used to model the structural dynamics of concrete beams after damage such as cracks [20] or voids [21]. However, after an earthquake there will often be large sections of concrete missing where the steel reinforcement is clearly visible. Therefore it is also useful to experimentally validate FEM models of reinforced concrete beams with and without a discontinuity (i.e. a large section of exposed reinforcement). This is carried out for larger numbers of bending and torsional modes than are commonly used to validate FEM for damage detection because using vibration to detect survivors within a collapsed building will potentially need to consider many more modes at frequencies up to a few kilohertz.

This paper investigates the potential to use normal contact stiffness to represent unbonded contacts between reinforced concrete beams using elastic springs for surface-to-surface and edge-to-surface contact conditions. Estimates for the spring stiffness do not appear to currently exist in the literature. The Finite Element Method (FEM) is used to create models for bending and torsional motion in the frequency range up to 3200 Hz. These are validated using Experimental Modal Analysis (EMA) with junctions of concrete beams. In each junction, the beams are stacked on top of each other without any bonding material and the interaction between the beams is modelled by using either linear elastic contacts (e.g. surface-to-surface junctions) or linear elastic springs (e.g. edge-to-surface junctions). Contact stiffness values are determined after model updating against experimental eigenfrequencies. The main aims are to experimentally validate FEM models of non-bonded concrete beams when in contact with each other (for beams with and without large discontinuities where there is only reinforcement), and to identify a suitable contact stiffness for surface-to-surface or edge-to-surface contact conditions.

2. Materials and methods

2.1 Reinforced concrete beams

The experimental samples consist of three reinforced concrete beams (C25/30, S500); these were all 2.4 m in length with a rectangular cross-section of 200×300 mm (see Figure 1). Beam 1 is reinforced with four longitudinal steel bars of 16 mm diameter whereas beams 2 and 3 are reinforced with eight

longitudinal steel bars of 16 mm diameter. The transverse reinforcement consists of 8 mm diameter stirrups placed at 200 mm centres along beams 1, 2 and 3. Beam 3 was designed to have a 100 mm wide discontinuity in the centre to simulate an (idealised) fracture that could occur in a collapsed building.

The density of the concrete for each beam was calculated by dividing the measured weight of the beams by the volume of concrete after extracting the weight of the steel reinforcement. The Young's modulus of the concrete was estimated after FEM model updating against the experimental results for the individual beams. For this reason the material properties of the beams are presented in Section 3.1.

2.2 Test setups

The beams were arranged so they could be tested individually and when forming a junction with surface-to-surface or edge-to-surface contact conditions. The term edge-to-surface is used where an edge on one beam makes a line connection across the surface area of the other beam.

2.2.1 Individual beams

Setups I1, I2 and I3 correspond to individual beams 1, 2 and 3 respectively when they are suspended from a crane using polyester slings. The slings were assumed to have negligible effect on the dynamic response such that the beams can be assumed to have free-free boundary conditions. This avoids additional uncertainty in the model updating process due to the modelling of boundary conditions. The beams were orientated so that bending wave motion occurred across the longer dimension of the cross-section (i.e. 300 mm thickness).

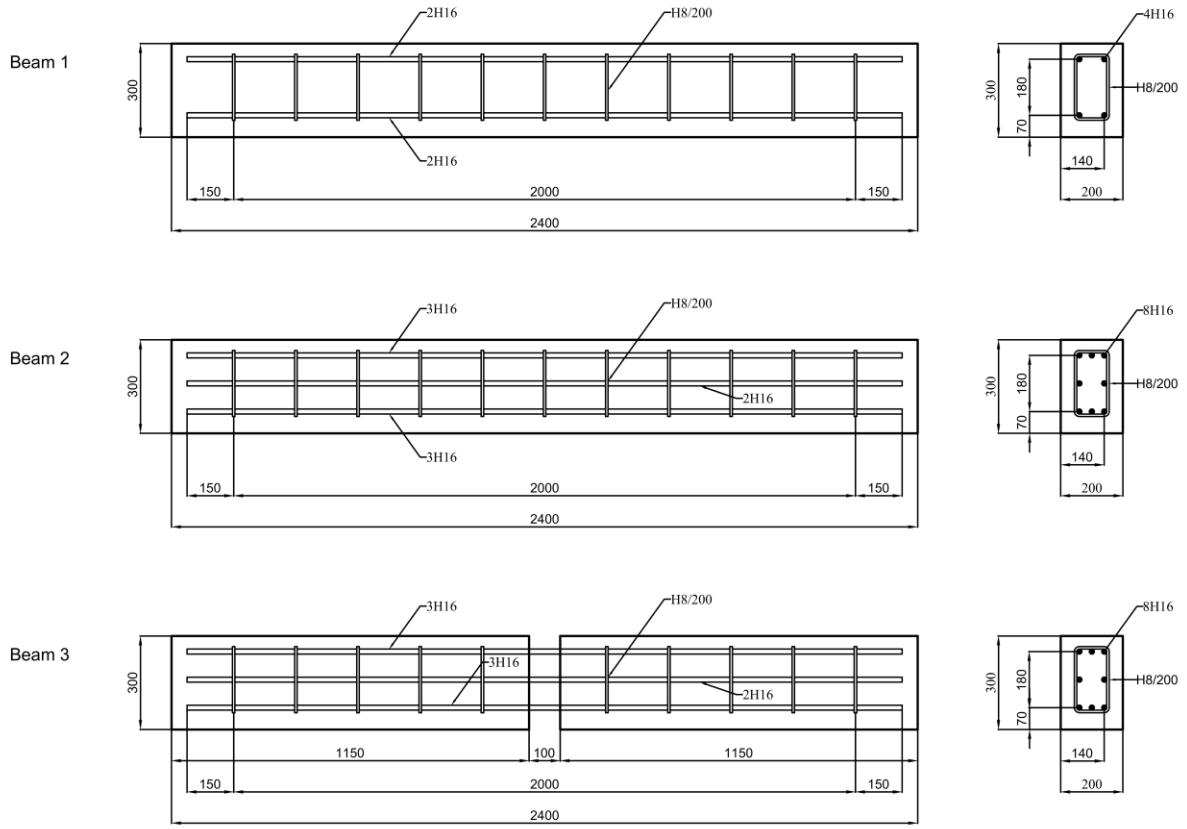

Figure 1. Reinforced concrete beam dimensions (units: millimetres).

2.2.2 Junctions

For the beam junctions shown in Figure 2 it was necessary to support the lowest beam, beam 1. Hence setup I4 was created with beam 1 orientated so that bending wave motion was across the shorter dimension of the cross-section (i.e. 200 mm thickness) and the lower surface of beam 1 rested upon a solid, square-section aluminium bar (25×25 mm) at each end. This aluminium bar rested on two concrete blocks (each 440×215×100 mm) stacked on top of each other; this was necessary to elevate them 200 mm above the ground for the operation of the crane that moved the beams.

The wave motion on the beams that formed the junction includes bending, torsional and longitudinal motion. However, only bending and torsional modes were considered in the analysis because longitudinal modes were not excited and longitudinal motion was not transferred by the normal contact stiffness between the beams.

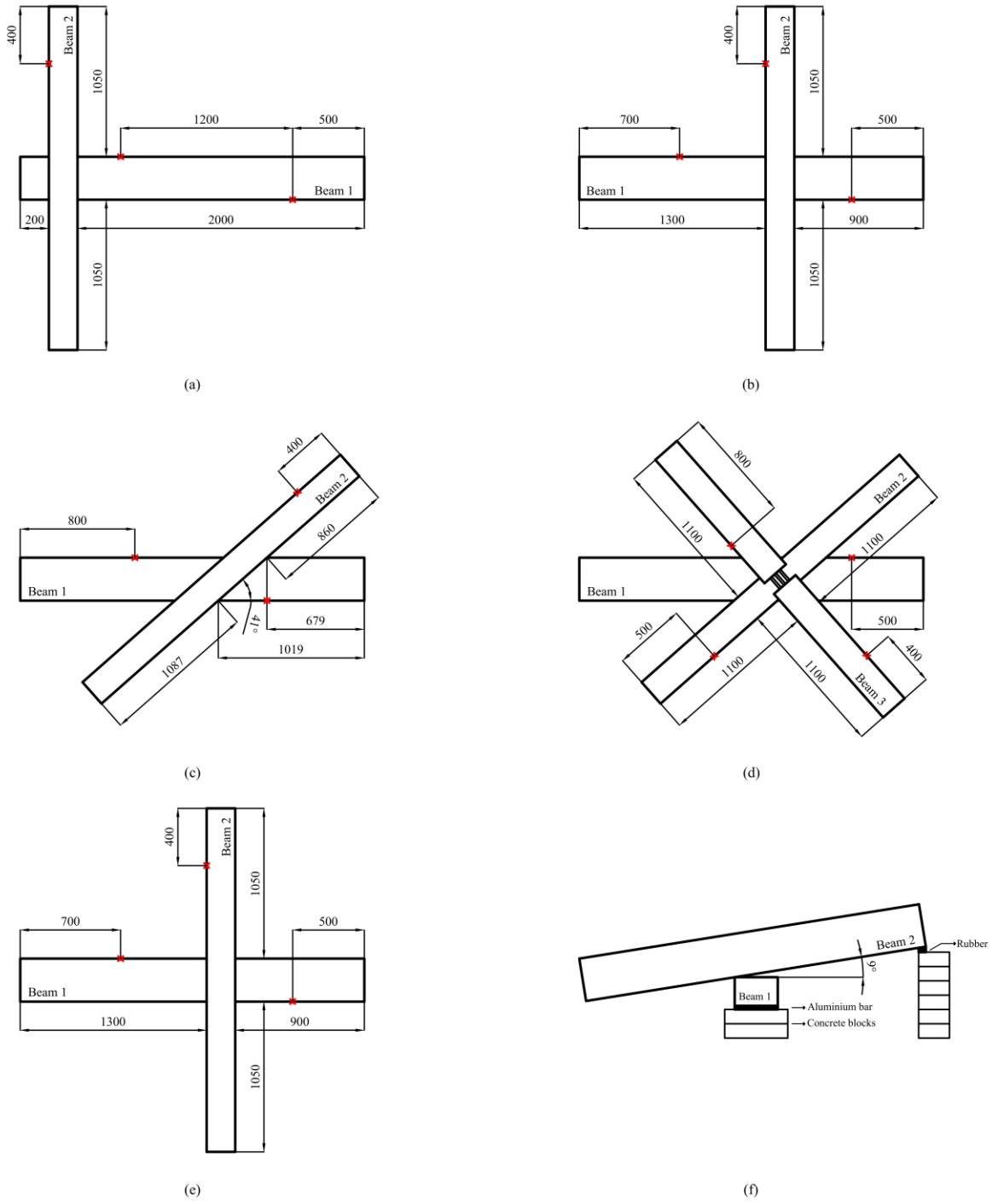

Figure 2. Test setups for the beam junctions: (a) J1, (b) J2, (c) J3, (d) J4, (e) J5 – Plan view and (f) J5 – Side view (units: millimetres).

2.2.2.1 Junctions of two beams (surface-to-surface contact)

Setups J1, J2 and J3 were formed by placing beam 2 on top of beam 1 in setup I4 to create a surface-to-surface contact condition. In setups J1 and J2, the angle between the beams is equal to 90° but the beams are in contact at different positions along the length (see Figure 2a and b). In Setup J3 the beams are at an angle of 41°; this was determined by the available space in the laboratory (see Figure 2c).

2.2.2.2 Junction of three beams (surface-to-surface contact)

In setup J4, beam 3 was placed on top of setup J3 to create a pile of three beams with surface-to-surface contact conditions (see Figure 2d). Beams 2 and 3 form a cross for reasons of stability because there are no supports at their ends.

2.2.2.3 Junction of two beams (edge-to-surface contact)

Setup J5 is identical to setup J2 except for the inclination angle of ≈9° between the two beams. To create edge-to-surface contact conditions, one end of beam 2 was elevated by 600 mm using six stacked concrete blocks with 30 mm thick rubber (60 mm length) to structurally isolate beam 2 from these blocks (see Figure 2e and 2f).

2.3 Experimental modal analysis

EMA is used to identify the material properties, damping and the modal characteristics of the individual beams and the beam junctions using FFT analysis with 1 Hz frequency lines. Brüel & Kjær Pulse Reflex software was used for signal processing and to carry out EMA. The beams were excited using an impact hammer (Brüel & Kjær Type 8200) and the response was measured using accelerometers (Brüel & Kjær Type 4371) both connected to a Nexus conditioning amplifier (Brüel & Kjær Type 2692) and a channel input module (Brüel & Kjær Type 3050-A-060). Table 1 shows the number of the accelerometers and the number of the excitation positions for each setup. Only out-of-plane acceleration was measured, except in setups I1, I2 and I3 where the response was measured in all three coordinate directions.

Table 1. Accelerometers and excitation positions for each test setup. In plane transducers excite/measure the response in a direction parallel to the ground plane. Out-of-plane transducers excite/measure the response in a direction normal to the ground plane.

Test setup	Description	No. of accelerometers		No. of excitation positions	
		In-plane	Out-of-plane	In-plane	Out-of-plane
I1	Beam 1 – sling supports	2	1	128	78
I2	Beam 2 – sling supports	2	1	128	78
I3	Beam 3 – sling supports	4	2	160	84
I4	Beam 1 – aluminium supports	-	3	-	100
J1	Junction of two beams (1&2) (surface-to-surface)	-	3	-	171
J2	Junction of two beams (1&2) (surface-to-surface)	-	3	-	171
J3	Junction of two beams (1&2) (surface-to-surface)	-	3	-	167
J4	Pile of three beams (1,2&3) (surface-to-surface)	-	4	-	242
J5	Junction of two beams (1&2) (edge-to-surface)	-	3	-	171

2.4 Finite element modelling

All finite element models used Abaqus software (Version 6.14) [22]. For the individual beams and the beam junctions, eigenvalue extraction used the Lanczos solver in the frequency range from 1 Hz to 3.2k Hz. For the beam junctions, mode-based, steady-state dynamic analysis was used to calculate vibration transmission between the beams in test setups J3, J4 and J5. Only the experimentally validated modes were included into the mode-based analysis using direct damping determined from the modal damping identified in the experimental work. The nodes of the top surface of the beams were excited by sequentially applying a unit load at the intersections of a 100 mm square grid which approximately corresponded to the hammer positions used in EMA.

2.4.1 Beams

FEM modelling of reinforced concrete beams commonly uses solid elements for the concrete and truss elements (e.g. see [23], [24], [25]) or beam elements [24] for the reinforcement. Truss elements have one degree of freedom per node, can sustain only axial deformation and cannot support bending wave motion [26]. For this reason they are not appropriate for modelling the steel reinforcement in the

damaged concrete beam of setups I3 and J4. Beam elements can model bending wave motion and therefore they are adopted for modelling the reinforced concrete members in this paper.

The concrete and the steel bars were modelled using solid element C3D20R (20 nodes) and beam element B32 (3 nodes) respectively. Both elements were selected to have interpolation functions of the same order (quadratic) to avoid a reduction in accuracy [22]. The element mesh had dimensions of 25 mm along the length of the beam and 20 mm over the beam cross-section to fulfil the requirement of at least six quadratic elements per bending wavelength.

2.4.2 Aluminium supports

The linear spring element, SPRING1 was used to approximate the elastic support that the aluminium square bars provide to beam 1 (see Figure 3). The stiffness of the springs was estimated to be 4.1E+05 N/m after model updating against the experimental results from setup I4. Numerical trials with different spring stiffness values were carried out until the lowest eigenfrequency from FEM and measurements were identical to one decimal place (193.8 Hz).

2.4.3 Rubber support

The linear spring element, SPRING1 (indicated by purple triangular markers in Figure 3) was selected from the element library of Abaqus to approximate the elastic support that the rubber material provides to beam 2 in setup J5. The stiffness of the springs was estimated to be 3236.8 N/m after measuring the stiffness of the rubber material according to the procedure described in ISO 9052-1 [27].

2.4.4. Surface-to-surface contact

The contact between the beams was modelled using the surface-to-surface contact algorithm of Abaqus/Standard and was defined to have elastic normal behaviour. When a contact is used in a linear perturbation step (such as in the eigenfrequency and steady-state analysis) the contact remains closed during the analysis when the starting condition is also closed [22]. Initial checks on the models confirmed that using a surface-to-surface contact with elastic normal behaviour during a linear perturbation step is equivalent to using an array of linear springs between the nodes of the two surfaces of the contact. The normal contact stiffness for each mode pair in setups J1, J2 and J3 was determined through model updating to give eigenfrequencies within 2% of the values identified with EMA.

2.4.5 Edge-to-surface contact

The linear spring element, SPRING2, was used to model the interaction between the edge nodes of beam 1 and the nodes along the lower surface of beam 2 in Setup J5 (see Figure 3). For every pair of coupled nodes, one horizontal and one vertical spring (acting in the X and Y directions respectively) were used to approximate a spring with a line of action normal to the lower surface plane of beam 2. The spring stiffness was the same as used for the surface-to-surface contact.

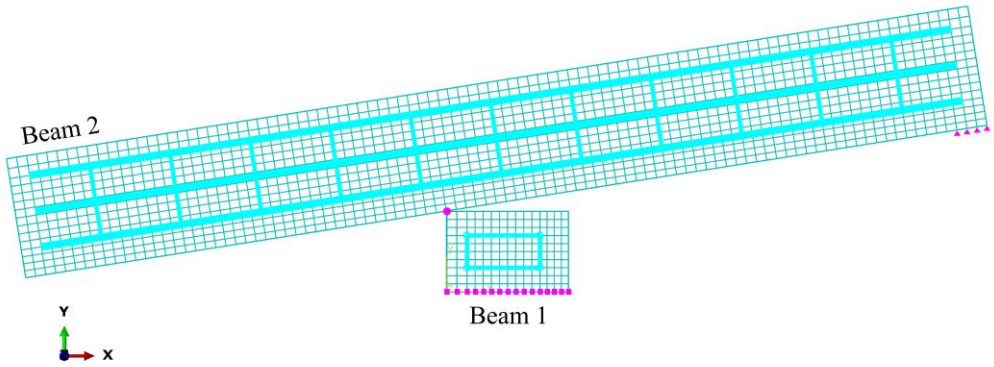

Figure 3. FEM model of test setup J5. Purple circular markers indicate SPRING2 elements used for modelling the interaction between beams 1 and 2. Purple square markers indicate SPRING1 elements that approximate the aluminium support. Purple triangular markers indicate SPRING1 elements that represent the rubber support.

2.4 Validation criteria used with data from the Experimental Modal Analysis

2.4.1 Mode shape criteria

The Modal Assurance Criterion (MAC) is used to assess the correlation between mode shapes from FEM and EMA using [28]

$$MAC(A,X) = \frac{\left|\{\varphi_X\}^{\mathrm{T}}\{\varphi_A\}^*\right|^2}{(\{\varphi_X\}^{\mathrm{T}}\{\varphi_X\}^*)(\{\varphi_A\}^{\mathrm{T}}\{\varphi_A\}^*)} \quad (1)$$

where X indicates the experiment, A indicates FEM, $\{\varphi_X\}$ and $\{\varphi_A\}$ are the column vectors of the degrees of freedom for the experimental and FEM mode shapes respectively, superscript T indicates the transpose and * is the complex conjugate.

An important limitation of MAC is that it is sensitive to large values and insensitive to small values [29]. Therefore, if one subset of the modal vector is significantly larger than the remaining subset of the modal vector, then the MAC value will be mainly determined by the former subset and any lack of correlation related to the latter will not be identified by MAC. In this paper, a subset is defined as the vector containing the degrees of freedom for each of the beams that form a junction. To overcome this problem, the Partial Modal Assurance Criterion (PMAC) [30] can be used to give insight into individual subsets of the modal vector by applying Eq. (1) to each subset separately. For two coupled beams it is feasible to consider the degrees-of-freedom on each beam as one subset. However, MAC and PMAC only describe correlation between the mode shapes and do not consider the relative response between different parts of the model. This is essential to assess the connection between the beams in this paper because it is necessary to check that the model correctly describes vibration transmission across the springs that are used to model the unbonded contact condition. The proposal here is to introduce an additional criterion, the Partial Modal Vector Ratio (PMVR) for which the results will be used to establish PMVR values that indicate close or reasonable agreement between FEM and measurements. PMVR is defined as the ratio in decibels of the squared modal vectors from EMA relative to FEM. For two subsets of the complete modal vector *i* and *j*, PMVR is given by

$$PMVR(A,X)_{i,j} = \left| 10\log_{10}\left(\left(\frac{\langle|\{\varphi_X\}_i|^2\rangle}{\langle|\{\varphi_X\}_j|^2\rangle}\right)\Big/\left(\frac{\langle|\{\varphi_A\}_i|^2\rangle}{\langle|\{\varphi_A\}_j|^2\rangle}\right)\right)\right| \tag{2}$$

where $\{\varphi_A\}$ and $\{\varphi_X\}$ are subsets of the modal vectors from FEM and EMA respectively.

2.4.2 Spatial-average transfer mobility ratio

Using point force excitation, a ratio of spatial-average transfer mobilities can be used to assess vibration transmission between two different beams in a junction. Using data from EMA or FEM, the spatial-average transfer mobility ratio, $YR_{ji,i}$, for two beams *i* and *j*, with force excitation on *i* is given by

$$YR_{ji,i} = 10\log_{10}\left(\frac{\left(\frac{1}{N}\sum_{k=1}^{N}\left|\frac{v_j}{F_i}\right|^2\right)}{\left(\frac{1}{N}\sum_{k=1}^{N}\left|\frac{v_i}{F_i}\right|^2\right)}\right) \tag{3}$$

where *v* is the velocity, *F* is the force, *m* is the mass, *N* represents the number of nodes in the FEM model or the number of accelerometer positions used in EMA.

3. Results and discussion

3.1 Individual beams

The Young's modulus of the concrete was estimated after updating the FEM model against the experimental results for individual beams 1 and 2 (and assuming nominally identical concrete properties for beams 2 and 3 which were cast on the same day). Numerical trials were carried out until the lowest eigenfrequency (bending motion) from FEM and measurements were identical to one decimal place (138.2 and 131.1 Hz for beams 1 and 2 respectively). Table 2 shows the material properties for the beams. The estimated Young's modulus for beam 1 is higher than beam 2 but within the range given for C25/30 concrete [31]; this might be caused by beam 1 being cast on a different day to beams 2 and 3. Material properties for steel and Poisson's ratio for concrete were taken from [31,32]. Average damping ratios for setups J3, J4 and J5 from EMA were 0.53, 0.49 and 0.49% respectively.

Table 2. Material properties of beams 1, 2 and 3.

Material	**Density, ρ (kg/m^3)**		**Young's modulus, E (N/m^2)**	**Poisson's ratio, ν (-)**
Concrete	Beam 1	2329	36875E+06	0.2
	Beam 2	2245	32475E+06	
	Beam 3	2235	32475E+06	
Steel	7800		200E+09	0.3

Comparison of FEM and experimental eigenfrequencies for setups I1 and I2 gave differences less than 5% for all mode pairs up to 3200 Hz whereas for setup I3 differences less than 5% were achieved for 25 out of 28 mode pairs. For setups I1 and I2, $MAC > 0.95$ was achieved for all bending and torsional modes up to 3200 Hz. For setup I3, six out of eight out-of-plane bending modes had $MAC > 0.95$ (NB Out-of-plane response is relevant to junction J4) although there was weaker agreement for the torsional modes with $MAC > 0.8$ for only three out of seven torsional modes.

3.2 Junctions of two beams (surface-to-surface contact)

3.2.1 Normal contact stiffness

Normal contact stiffness values were determined from model updating of the FEM model against EMA for the first 24 modes in each of the setups J1, J2 and J3. These are shown in Table 3 in terms of the mean, minimum and maximum values. Due to the relatively wide range of values for the modes and the significantly different mean values for setup J2, the validity of the FEM models was assessed using the mean stiffness for each individual setup (J1, J2 and J3) in the following sections.

Table 3. Normal contact stiffness values determined from model updating for the surface-to-surface contacts in setups J1, J2 and J3.

Test setup	Number of modes	Contact area (m^2)	Normal contact stiffness (N/m)		
			Mean	Minimum	Maximum
J1	22	0.06	7.6E+08	5.1E+05	3.9E+09
J2	22	0.06	4.5E+08	1.5E+06	2.2E+09
J3	23	0.09	7.5E+08	5.0E+05	4.3E+09

3.2.2 Eigenfrequencies

Figure 4 compares FEM and experimental eigenfrequencies for setups J1, J2 and J3. Close agreement was achieved with differences less than 5% for the majority of mode pairs from 700 to 3200 Hz. The three setups have similar eigenfrequencies because global modes of the setups are partly determined by eigenfrequencies of the individual isolated beams, and these beams are the same in each of these setups.

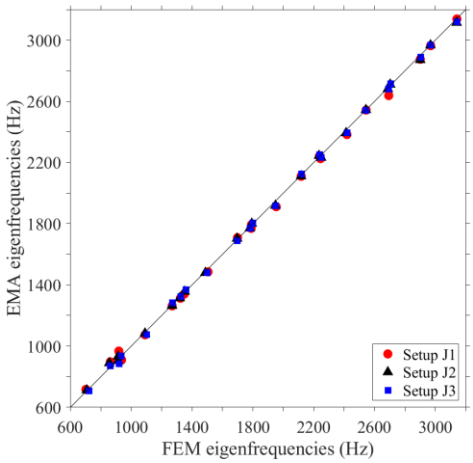

Figure 4. Comparison of FEM and experimental eigenfrequencies for test setups J1, J2 and J3.

3.2.3 Mode shapes

In this section, setup J3 is shown as an example to assess the FEM model in terms of MAC, PMAC and PMVR because the other two setups give similar findings. Correlation between EMA and FEM is shown using MAC in Figure 5. Note that only bending and torsional modes were included in the validation procedure of the FEM models. While there is close agreement ($MAC > 0.8$) for the first two modes there was poor agreement for modes three, four and five. Close agreement ($MAC > 0.8$) was achieved above the first five global modes (i.e. between 1000 and 3200 Hz) for 17 of the mode pairs.

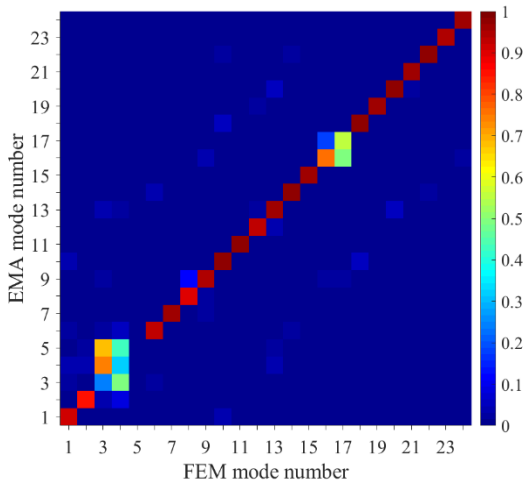

Figure 5. MAC values for the FEM model of test setup J3.

For setup J3 that comprises two beams, Figure 6 allows comparison of MAC and PMAC for beams 1 and 2. Note that there is no data for the fifth mode pair as this pair was not identifiable. It is seen that for each mode pair there is often a PMAC value for one beam that is higher or similar to the MAC, and one PMAC value for the other beam that is lower than the MAC. The reason for this is the sensitivity of MAC to large values in the modal vector. Note that only seven of the 24 mode pairs had $PMAC > 0.8$ for both beams. The global modes of the coupled beams are related to the local modes of each isolated beam where one or both beams have an identifiable modal response that is similar to the local mode shape. Hence there are some global modes where only one beam has a clear modal response and the other has a low response; in this situation, the modal vectors of the former beam primarily determine the MAC and the influence of the other beam will be negligible. For example, in Figure 7a the modal

vectors of beam 2 determine the MAC value of the mode pair 12, whereas in Figure 7b the MAC value of mode pair 18 is determined by the modal vectors of beam 1.

Figure 8 compares FEM and experimental results for setup J3 using PMVR (note that the empty column indicates that mode pair 5 was not identified). When introducing this new descriptor in section 2.5.1 it was noted that a range of acceptable values could not be assigned *a priori*. A value of 0 dB would indicate complete correlation between EMA and FEM. However, as the contact condition is modelled using a single contact stiffness value it is expected that low values, such as between 0 and 2 dB, might occur for a few mode pairs. In this paper the application considers the response in frequency bands; hence the velocity level difference between two beams when one is excited by a point force will be determined by more than one mode pair. For this reason, two criteria are proposed based on the results from all beam junctions, close agreement being defined as $PMVR \leq 5$ dB (33% of mode pairs) and reasonable agreement being 5 dB < $PMVR \leq 10$ dB (25% of mode pairs). Only 38% of mode pairs had $PMVR > 10$ dB. These results indicate that the interaction model in FEM is appropriate.

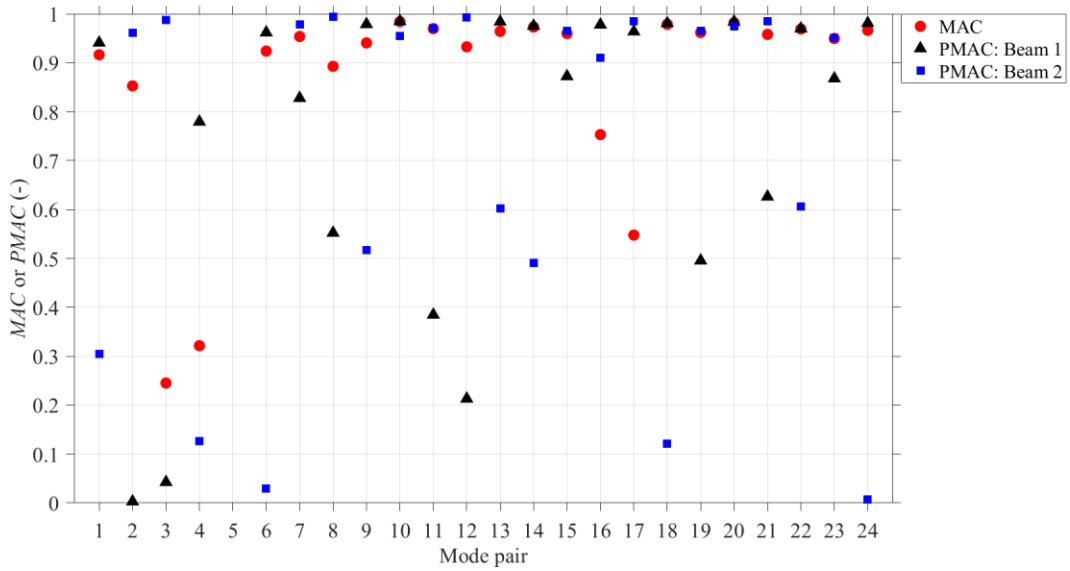

Figure 6. PMAC values for the FEM model of test setup J3.

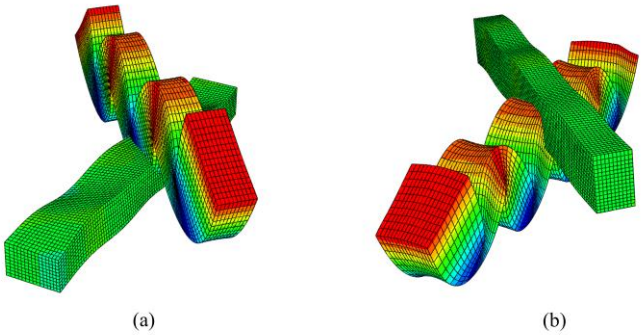

Figure 7. FEM mode shapes of test setup J3: (a) Mode 12 at 1782.3 Hz and (b) Mode 18 at 2418.8 Hz.

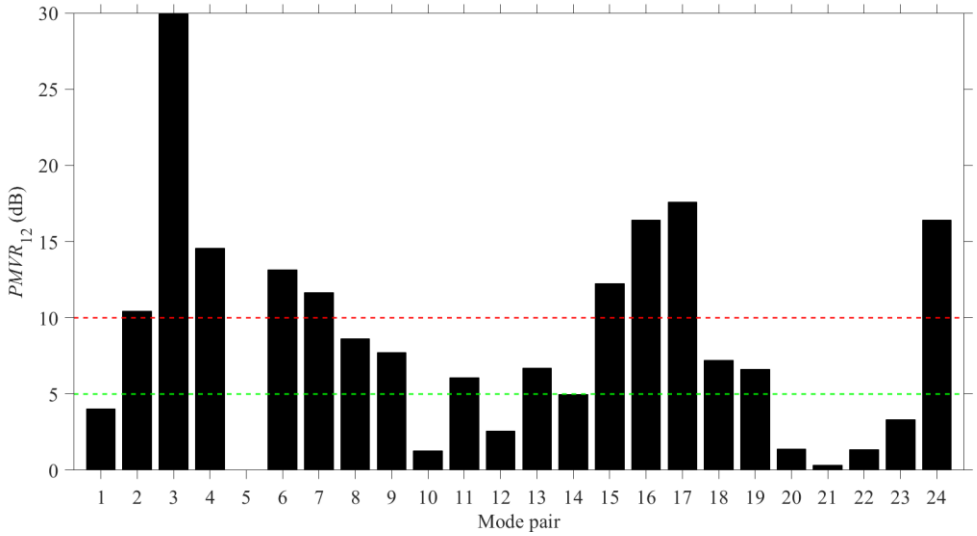

Figure 8. PMVR values for the FEM model of test setup J3. Green and red dashed lines indicate levels of 5 dB and 10 dB respectively.

3.2.4 Spatial-average transfer mobility ratio

Setup J3 is now used to illustrate features of the spatial-average transfer mobility ratio. Figures 9a and 9b allow comparison of these ratios from FEM and measurements when a point force is applied to beams 1 and 2 respectively. Below 650 Hz there are only rigid body modes; hence results are shown above 650 Hz using 17 frequency bands with a 150 Hz bandwidth to simplify the comparison.

The results for FEM and measurements have similar curves, except in the lowest and highest frequency bands, with the average difference being 2.4 dB. This indicates that FEM can provide reasonable estimates of vibration transmission between coupled beams by using a single value for the contact

stiffness. The next section considers a three beam junction (setup J4) and combines the stiffness values determined from setups J1, J2 and J3 by treating them as a sample of the population in order to identify a single contact stiffness value that could be used in FEM models for any concrete elements in a collapsed building.

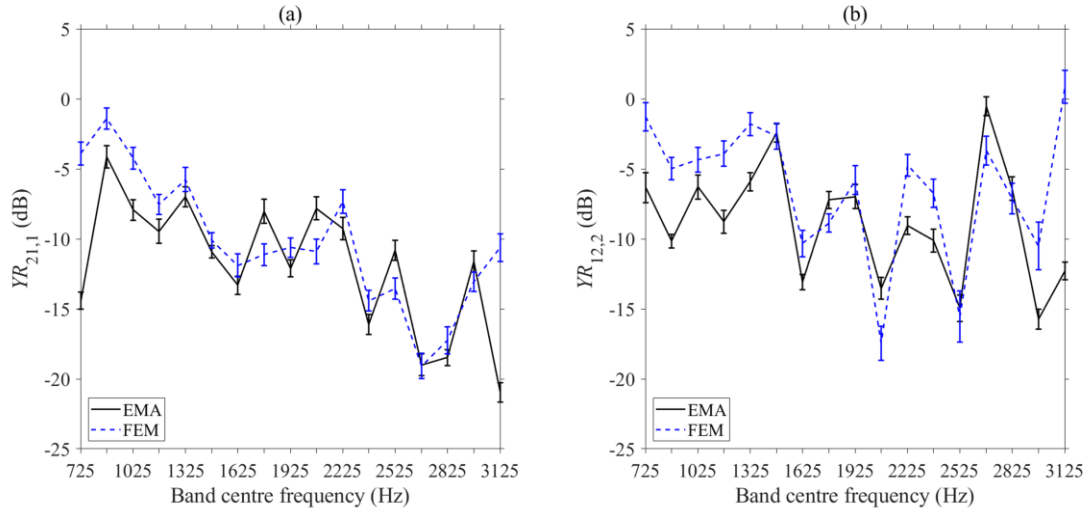

Figure 9. Spatial-average transfer mobility ratio for test setup J3: (a) $YR_{21,1}$ and (b) $YR_{12,2}$.

3.3 Junction of three beams (surface-to-surface contact)

This section aims to identify and assess the use of a single, representative value for the contact stiffness that could be used to model collapsed buildings where there is a high level of uncertainty in the modal properties of the fragmented structure as well as the position of the contact and its surface area.

3.3.1 Normal contact stiffness derived from model updating

In Section 3.2, model updating with setups J1, J2 and J3 resulted in 67 individual values for the normal contact stiffness. It is now assumed that these values represent a sample from a population for which a representative average value could be identified that has general application to two coupled beams. The contact stiffness values for each mode were divided into classes and a probability distribution was fitted to the data using the MATLAB distribution fitter toolbox [33]. The stiffness values are sub-divided into nine bins with a width of 4.78E+08 N/m for which the fitted probability distribution is a lognormal distribution (see Figure 10) with a mean value of 7.038E+08 N/m. As the first bin contains 66% of the values it is also feasible to consider the mean of the values in this bin which was 8.77E+07 N/m.

Previous work [34] has also identified that lognormal distributions describe structural coupling parameters between stiff, heavy structures (i.e. concrete) where there are relatively few modes; this applies to the coupling situation assessed in this paper with the concrete beams.

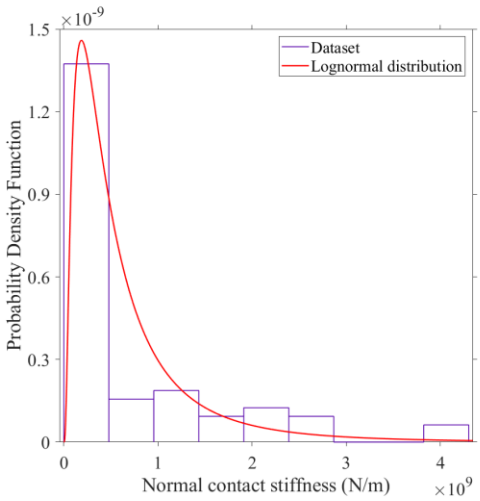

Figure 10. Lognormal probability distribution fitted to the dataset of the normal contact stiffness.

3.3.2 Eigenfrequencies

An assessment of FEM is now made through comparison with EMA when the normal contact stiffness is (a) the mean value of the first bin, i.e. 8.77E+07 N/m (referred to as FEM model No.1) and (b) the mean value of the lognormal distribution, i.e. 7.038E+08 N/m (referred to as FEM model No.2). Figure 11 allows comparison of models No.1 and 2 against EMA for setup J4. Both FEM models show close agreement with differences less than 5% for most mode pairs. Considering only the first eight mode pairs, the average difference (3.7%) is lower for model No.1 than No.2 (6.0%). While the normal contact stiffness affects the global eigenfrequencies below 1200 Hz, both models have similar eigenfrequencies above 1200 Hz (average differences are 0.98% and 1.3% for models No.1 and 2 respectively). This indicates that global eigenfrequencies of the junction are mainly determined by eigenfrequencies of individual beams rather than their interaction.

3.3.3 Mode shapes

MAC results for Setup J4 are shown in Figures 12a and 12b. For the first eight correlated mode pairs (i.e. below 1200 Hz), *MAC*>0.8 for seven mode pairs with FEM model No.1 but only three mode pairs with No.2. Above the eighth mode (i.e. between 1200 and 3200 Hz), both FEM models showed equally

close agreement with *MAC* > 0.8 for 17 of the 32 mode pairs. In terms of PMAC, neither of the FEM models had *PMAC* > 0.8 for all three beams (see Figures 13a and 13b). This issue with one or two of the individual beams was not detected with MAC because (as discussed in section 3.2.3) the MAC value is primarily determined by the modal vectors of one beam.

In terms of PMVR, close agreement (≤ 5 dB) was achieved for 16% and 29% of the mode pairs from models No.1 and 2 respectively. It is seen that for model No.1, many PMVR values are >10 dB (see Figures 14a, b and c). Hence, whilst model No.1 had higher MAC values than No.2, PMVR indicates that model No.2 gives an improved representation of the interaction between the coupled beams.

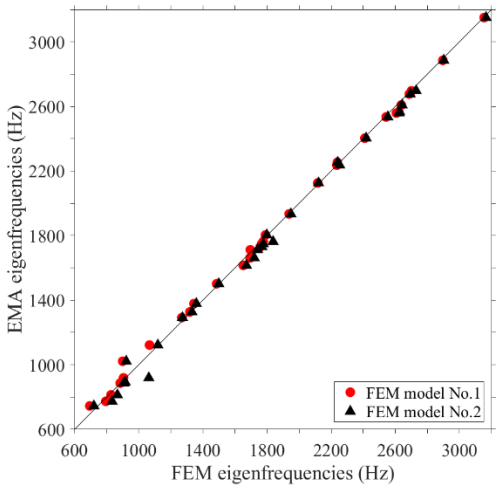

Figure 11. Comparison of FEM model No.1 and 2 against experimental eigenfrequencies for test setup J4.

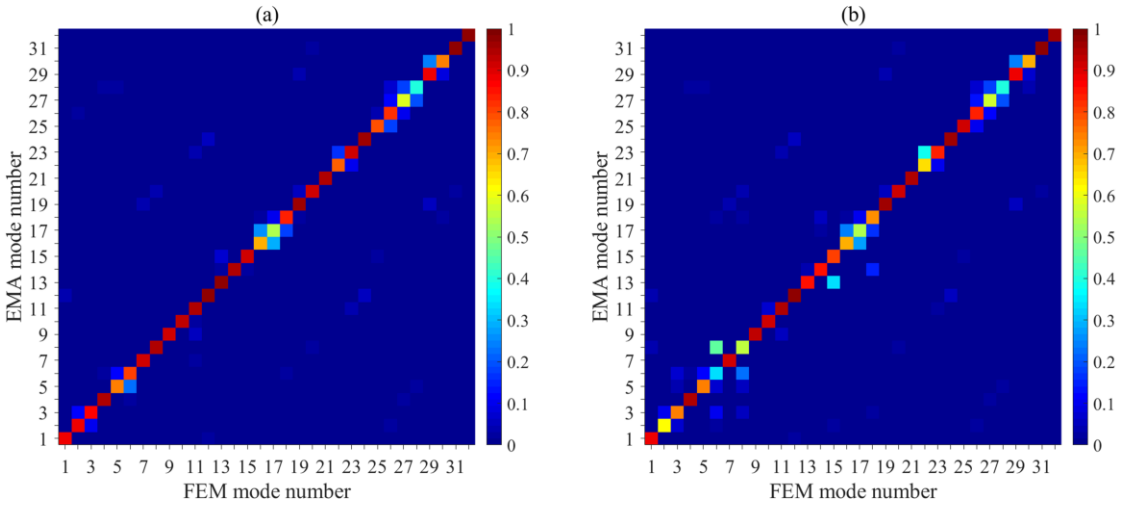

Figure 12. MAC values for test setup J4: (a) FEM model No.1 and (b) FEM model No.2.

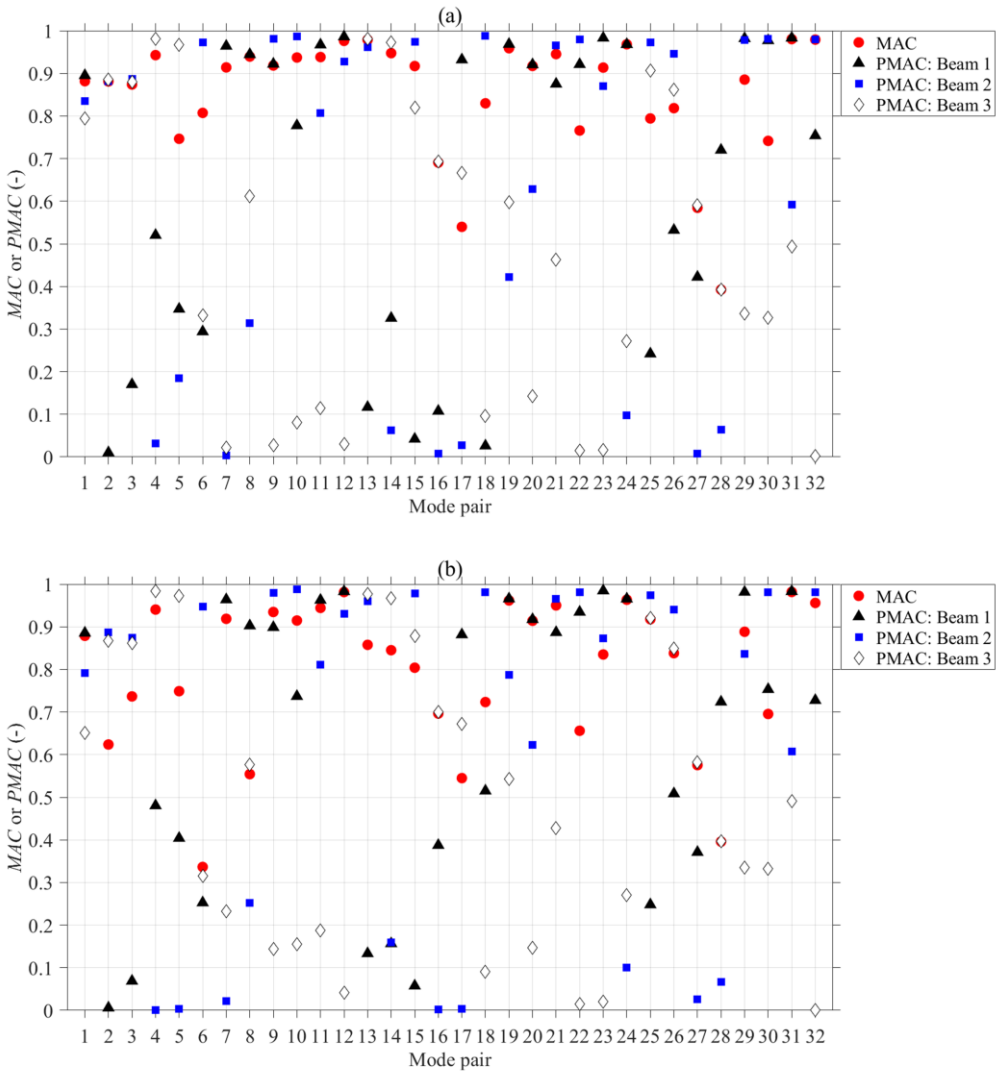

Figure 13. PMAC values for test setup J4: (a) FEM model No.1 and (b) FEM model No.2.

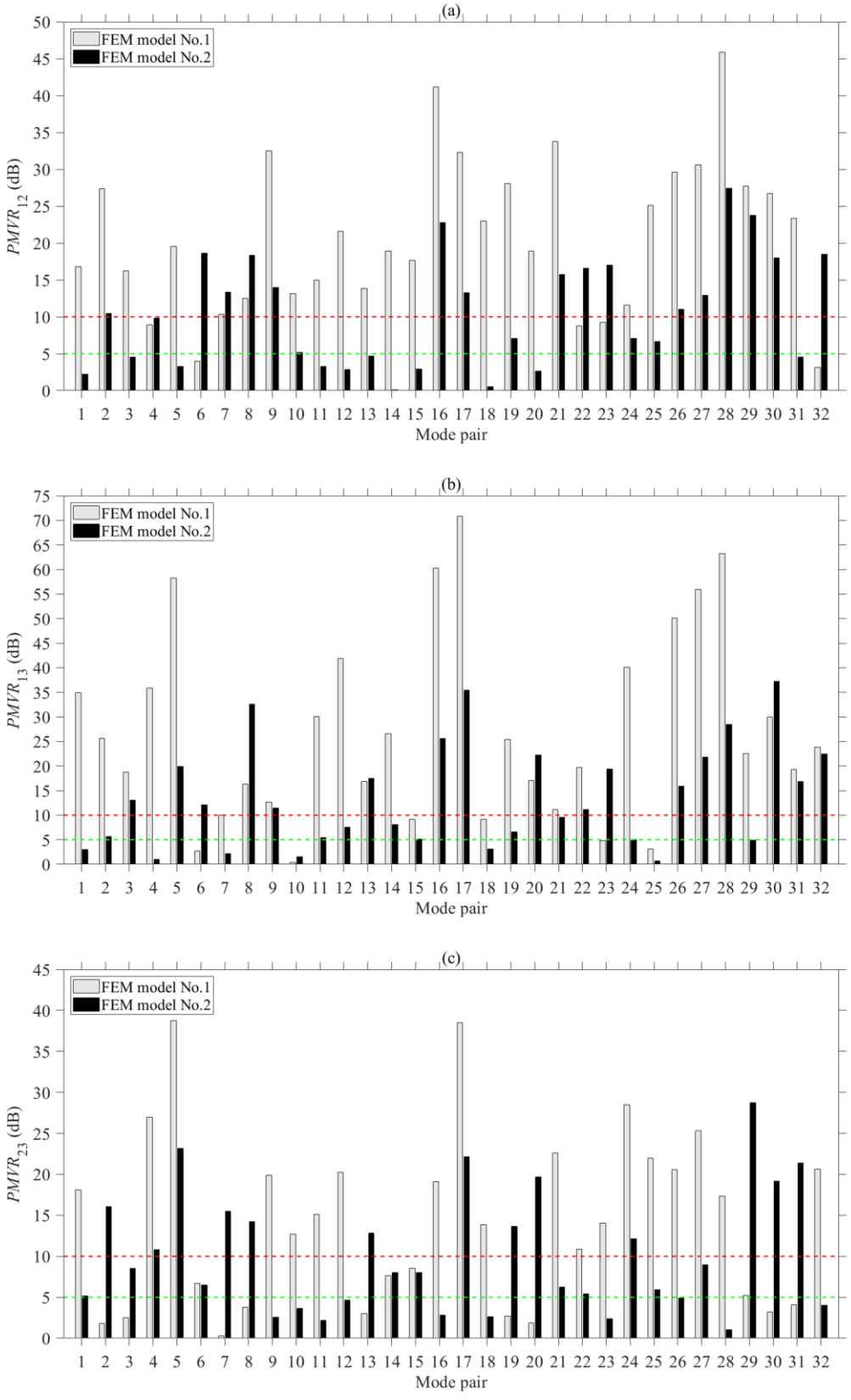

Figure 14. PMVR for FEM models No.1 and 2 with test setup J4: (a) $PMVR_{12}$, (b) $PMVR_{13}$ and (c) $PMVR_{23}$.

3.3.4 Spatial-average transfer mobility ratio

Figure 15 allows comparison of FEM models No.1 and No.2 with EMA for the beams in setup J4. When the force is applied to beam 1 (Figures 15a and b), model No.2 shows closest agreement with EMA (differences less than 4 dB) whereas No.1 was offset with differences up to 12 dB on average.

When the force is applied to beam 2 (Figure 15c) or beam 3 (Figure 15e), model No.2 also shows significantly closer agreement with EMA than No.1. However, Nos. 1 and 2 show reasonable agreement when the force is applied to beam 2 (Figure 15d) or beam 3 (Figure 15f) and the velocity response is measured on beams 2 and 3. This indicates that the choice of contact stiffness might be less critical when the area connection is reduced, in this case the reduced area is due to the discontinuity in beam 3.

In general, model No.2 is significantly better than No.1 for modelling vibration transmission between the beams in setup J4. Therefore, the mean value of the lognormal distribution provides a better approximation of the normal contact stiffness to model the dynamic behaviour of beam junctions where the beams are connected with a surface-to-surface contact. The next section assesses the potential of using this normal contact stiffness value in beam junctions with edge-to-surface contact conditions.

The FEM model that most closely represented the physical situation was identified by PMVR but not by MAC. MAC led to a misleading validation by indicating that model No.1 was more accurate than No.2. As MAC is very sensitive to large values, any correlation problem caused by the interaction between the beams is not reflected in its value. For this reason, it is proposed here that PMVR is a computationally efficient supplement to MAC when validating FEM models where structural components are coupled by elastic connections of unknown stiffness.

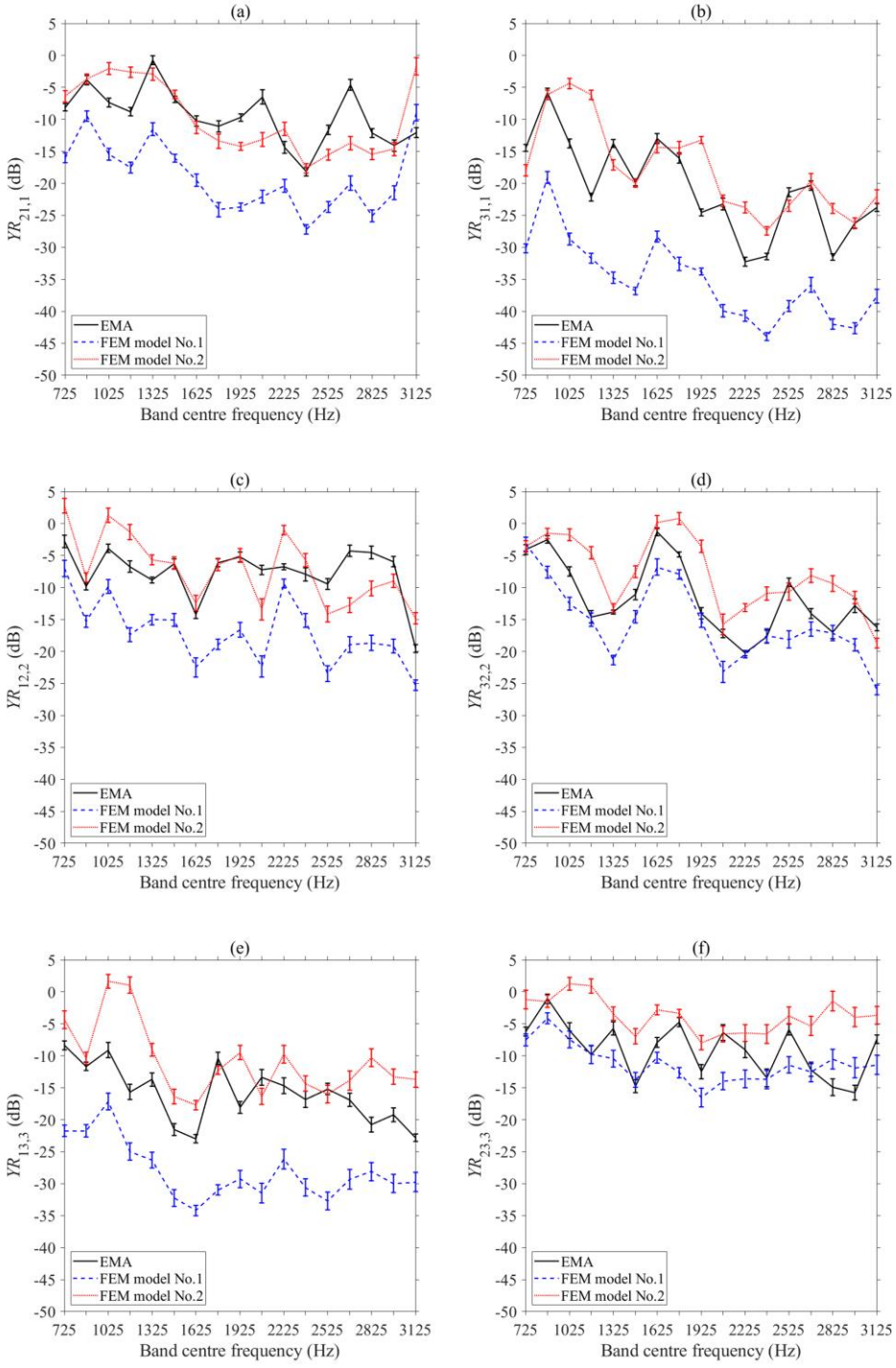

Figure 15. Spatial-average transfer mobility ratios for test setup J4: (a) $YR_{21,1}$, (b) $YR_{31,1}$, (c) $YR_{12,2}$, (d) $YR_{32,2}$, (e) $YR_{13,3}$ and (f) $YR_{23,3}$.

3.4 Junction of two beams (edge-to-surface contact)

Based on the findings in the previous section, only one FEM model is used in this section. This uses the mean value of the lognormal distribution for the normal contact stiffness.

3.4.1 Eigenfrequencies

Figure 16 compares FEM and experimental eigenfrequencies for setup J5. Close agreement was achieved with differences less than 3% for mode pairs in the frequency range from 700 to 3200 Hz.

3.4.2 Mode shapes

In terms of MAC, close agreement ($MAC > 0.8$) was achieved for 21 out of 23 mode pairs with reasonable agreement ($MAC > 0.7$) for mode pairs 8 and 23 (see Figure 17). Beams 1 and 2 have $PMAC > 0.8$ for 15 out of the 23 mode pairs (see Figure 18). PMAC results were higher than occurred with the surface-to-surface contact which indicates that the reduced contact area with an edge-to-surface contact introduces lower errors when modelling the coupling. In terms of PMVR, close agreement ($PMVR \leq 5$ dB) was achieved for 22% of the mode pairs with reasonable agreement (5 dB < $PMVR \leq 10$ dB) for 52% of the mode pairs with 26% of mode pairs had $PMVR > 10$ dB (see Figure 19).

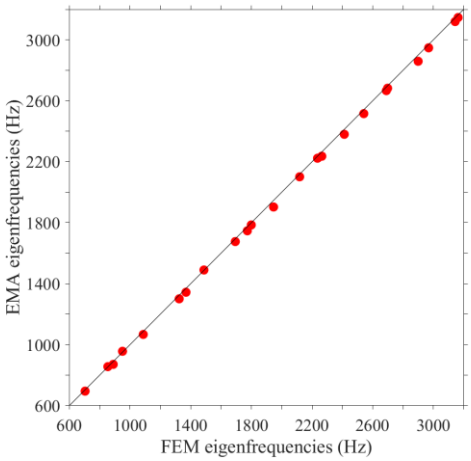

Figure 16. Comparison of FEM against experimental eigenfrequencies for test setup J5.

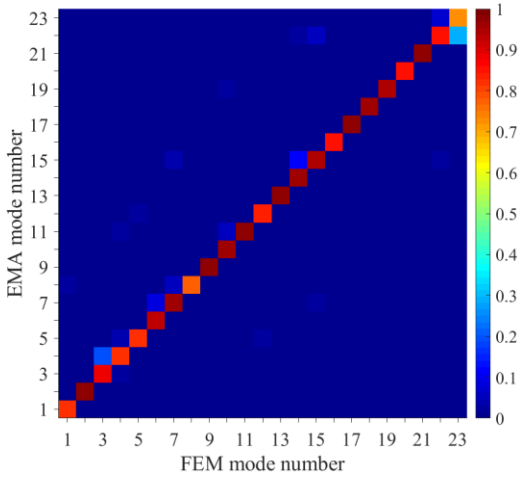

Figure 17. MAC values for the FEM model of test setup J5.

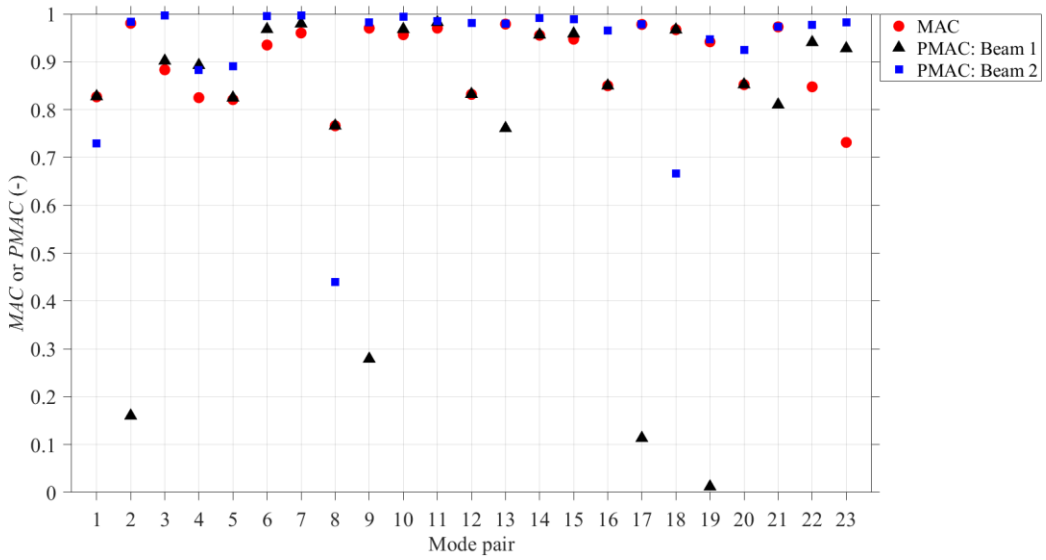

Figure 18. PMAC values for the FEM model of test setup J5.

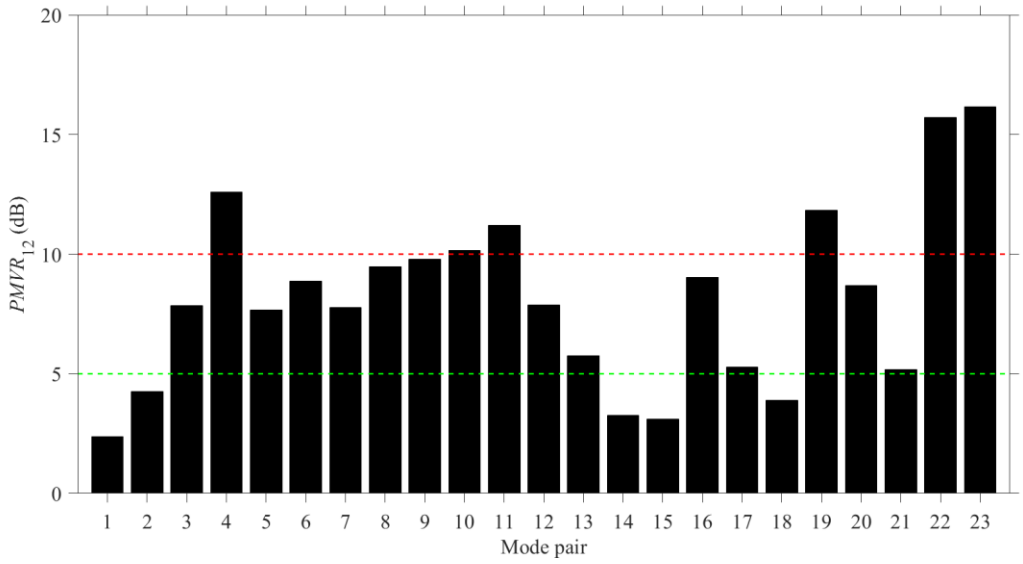

Figure 19. PMVR values for the FEM model of test setup J5.

3.4.3 Spatial-average transfer mobility ratio

Figures 20a and b allow comparison of FEM and EMA in terms of the spatial-average transfer mobility ratio for setup J5. For a point force applied to beam 1 (Figure 20a) and beam 2 (see Figure 20b), FEM and EMA show reasonable agreement within 4 dB on average. This confirms that the mean value of the lognormal distribution can be used for the contact stiffness in FEM models where the beams are connected by an edge-to-surface contact.

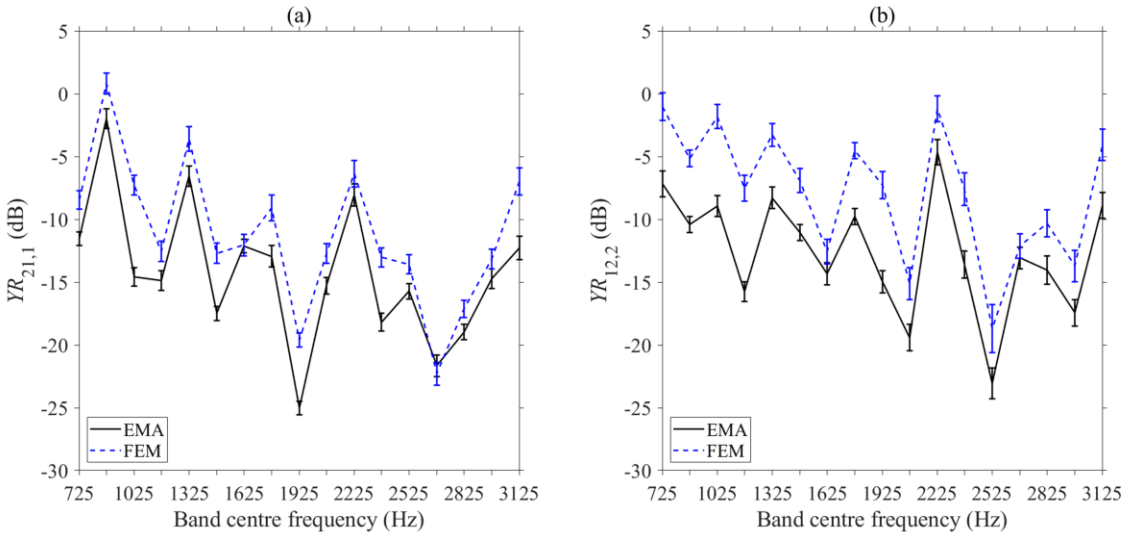

Figure 20. Spatial-average transfer mobility ratio for test setup J5: (a) $YR_{21,1}$, (b) $YR_{12,2}$.

4. Conclusions

FEM models have been developed and validated with experimental modal analysis for beams connected with surface-to-surface and edge-to-surface contact conditions. These models were validated in terms of eigenfrequencies, mode shapes and spatial-average response. It was shown that the interaction between the beams could be approximated using a normal contact stiffness. This stiffness showed some dependence on the modal response with values forming a lognormal distribution. It was shown that the mean value of this lognormal distribution could be used to approximate the contact stiffness in FEM models of beams junctions with surface-to-surface or edge-to-surface contact conditions.

For concrete beams that are stacked on top of each other without any rigid bonding material it was shown that MAC is not adequate to assess the validity of the FEM model as this can lead to misleading results. Using PMAC for these beams, it was shown that MAC was mainly determined by the modal vectors of one beam whereas the contribution of the other beam(s) to the MAC value was negligible. To overcome the shortcomings of MAC when validating FEM models of structural coupling between elastic systems using spring connectors to model the unbonded contact condition, an additional criterion, the Partial Modal Vector Ratio was introduced. This criterion allowed identification of the FEM model that gave the most appropriate representation of the interaction between the coupled beams.

Compared to running FEM models with applied loads to assess vibration transmission between the coupled beams, PMVR is a time efficient approach and can be used as a supplementary criterion to MAC to identify potential correlation problems caused by the interaction of the beams.

Acknowledgments

The authors are grateful for the funding provided by the EPSRC and ESRC Centre for Doctoral Training in Quantification Management of Risk & Uncertainty in Complex Systems and Environments at the University of Liverpool. The authors are also very grateful to Dr Gary Seiffert (Acoustics Research Unit) for all his help with the experimental set-ups.

References

[1] Zhao B, Taucer F, Rosseto T. Field investigation on the performance of building structures during the 12 May Wenchuan earthquake in China. Eng Struct 2009;31:1707-1723.

[2] Sezen H, Whittaker AS, Elwood KJ, Mosalam KM. Performance of reinforced concrete buildings during the August 17, 1999 Kocaeli, Turkey earthquake, and seismic design and construction practice in Turkey. Eng Struct 2003;25:103-114.

[3] Saatcioglu M, Ghobarah A, Nistor I. Performance of structures in Indonesia during the December 2004 great Sumatra earthquake and Indian ocean tsunami. Earthq Spectra 2006;22:S295-S319.

[4] Bartels SA and VanRooyen MJ. Medical complications associated with earthquakes. The Lancet, 2012;379(9817):748-757.

[5] Macintyre AG, Barbera JA and Smith ER. Surviving collapsed structure entrapment after earthquakes: A "Time-to-Rescue" analysis. Prehosp Disaster Med 2006;21(1):4-19.

[6] Friedman M, Haddad Y and Blekhman A. ACOUFIND: Acoustic Ad-Hoc Network System for Trapped Person Detection. IEEE International Conference on Microwaves, Communications, Antennas and Electronic Systems, Tel Aviv, 2015.

[7] Bäckström C-J and Christofferson N. Urban search and rescue - an evaluation of technical search equipment and methods. Lund University, Lund, 2006. LUTVDG/TVBB-5197-SE.

[8] Ervin EK. Vibro-impact behavior of two orthogonal beams. J Eng Mech 2009;135:529-537.

[9] Zhou F, Mosalam KM, Nakashima M. Finite-element analysis of a composite frame under large lateral cyclic loading. J Struct Eng 2007;133:1018-1026.

[10] Filippoupolitis M and Hopkins C. Structural dynamics of a dowelled-joist timber floor in the low-frequency range modelled using finite element simulation. Eng Struct 2017;148:602-620.
[11] Martinelli P, Galli A, Barazzetti L, Colombo M, Felicetti R, Previtali M, Roncoroni F, Scola M, Di Prisco M. Bearing capacity assessment of a 14th century arch bridge in Lecco (Italy). Int J Archit Herit 2018;12:237-256.
[12] Marwala T. Finite-element model updating using computational intelligence techniques. Springer; 2010, ISBN 978-1-84996-323-7.
[13] Seelig JM, Hoppman WH. Normal mode vibrations of systems of elastically connected parallel bars. J Acoust Soc Am 1964;36:93-99.
[14] Rao SS. Natural vibrations of systems of elastically connected Timoshenko beams. J Acoust Soc Am 1974;55:1232-1237.
[15] Oniszczuk Z. Free transverse vibrations of elastically connected simply supported double-beam complex system. J Sound Vib 2000;232:387-403.
[16] Farrar CR, Doebling SW and Nix DA. Vibration–based structural damage identification. Philos T R Soc A 2001;359(1778):131-149.
[17] Perera R, Huerta C and Orquı JM. Identification of damage in RC beams using indexes based on local modal stiffness. Constr Build Mater 2008;*22*(8):1656-1667.
[18] Xu B and Gong X. Damage detection of reinforced concrete columns based on vibration tests. Earth and Space 2010: Engineering, science, construction, and operations in challenging environments 2010. 2321-2329.
[19] Jaishi B and Ren WX. Damage detection by finite element model updating using modal flexibility residual. J Sound Vib 2006;290(1-2):369-387.
[20] Mazaheri H, Rahami H and Kheyroddin A. Static and dynamic analysis of cracked concrete beams using experimental study and finite element analysis. Period Polytech-Civ 2018;62(2):337-345.
[21] Dawari VB and Vesmawala GR. Modal curvature and modal flexibility methods for honeycomb damage identification in reinforced concrete beams. Procedia Eng 2013;51:119-124.
[22] Abaqus 6.14 Documentation and User Manual. Providence, Rhode Island, USA;2014. Dassault Systèmes Simulia Corporation.
[23] Pešić N, Živanović S, Dennis J, Hargreaves J. Experimental and finite element dynamic analysis of incrementally loaded reinforced concrete structures. Eng Struct 2015;103:15-27.
[24] Earij A, Alfano G, Cashell K, Zhou X. Nonlinear three–dimensional finite–element modelling of reinforced–concrete beams: Computational challenges and experimental validation. Eng Fail Anal 2017;82:92-115.
[25] Ožbolt J and Sharma A. Numerical simulation of reinforced concrete beams with different shear reinforcements under dynamic impact loads. Int J Impact Eng 2011;38:940-950.
[26] Hutton DV. Fundamentals of Finite Element Analysis. 1st ed. New York: McGraw-Hill, 2004.

[27] ISO 9052-1:1989 Acoustics – Determination of dynamic stiffness – Part 1: Materials used under floating floors in dwellings, International Organization for Standardization.
[28] Ewins DJ. Modal testing: theory, practice and application. 2nd ed. Research Studies Press Ltd; 2000, ISBN 0-86380-218-4.
[29] Allemang RJ. The modal assurance criterion – Twenty years of use and abuse. Sound Vib 2003;14-21.
[30] Heylen W, Janter T. Extensions of the modal assurance criterion. J Vib Acoust 1990;112:468-472.
[31] Bamforth P, Chisholm J, Gibbs J, Harrison T. Properties of concrete for use in Eurocode 2. The Concrete Centre. 2008. ISBN 978-1-904482-39-0.
[32] Mosley B, Bungey J, Hulse R. Reinforced concrete design to Eurocode 2. Palgrave Macmillan. 2012. ISBN 978-0-230-30285-3.
[33] MATLAB R2018b. Natick, Massachusetts; 2018. The Mathworks Inc.
[34] Hopkins C. Statistical energy analysis of coupled plate systems with low modal density and low modal overlap. J Sound Vib 2002;251(2):193-214.